Elastic modeling by phase-shift cascade with scattering matrix control

Chanpen Silawongsawat and Gary F. Margrave

SUMMARY

A new numerical technique for elastic modeling in a stratified medium is introduced and applied in the following procedure. A surface point source emits a pulsed cylindrical P (or S) wave in a stratified medium (*x*-*z* plane). Using Fourier analysis, the cylindrical wave is decomposed into a sum of harmonic plane waves and the numerical operations are defined in *f*-*k* domain. The technique iteratively uses phase shift extrapolation in depth to propagate elastic potentials and modified-for-potential Zoeppritz equations to compute reflection, transmission and conversion coefficients. All multiples and mode conversions are generated and may be turned off via scattering-matrix modification. The spectral result is obtained by cascading each plane wave (each *f*-*k* component) through a computational grid and, then, transformed to yield 2-D elastic seismograms in time-space domain. Options for free surface effects and displacement conversions are made before the inverse Fourier transformation.

The program is built in the Matlab environment and illustrated with three simple models. The results from two single-interface models show the method produces head waves. The cylindrical PP reflection coefficients extracted from synthetic data are shifted and smoothed compared to the plane wave analytic from Zoeppritz equations. Multiples and converted modes from another model are very realistic though there are some algorithmic artifacts have not been completely solved yet. The method works and is fast and stable. It produces seismograms with reasonable agreement to theory and with some interesting characteristics which need to be investigated more. The program itself has great potential for many extensions and applications including 3-D synthetics, anisotropy, anelasticity and wave effects at any specific range of depth.

INTRODUCTION

There are many approaches to the problem of computing a synthetic seismogram representing the recording of an elastic wavefield. These include: complete, analytical solutions like the Cagniard-De Hoop method (Aki and Richards, 1980, p224), semi-analytical methods like the reflectivity method (Fuchs and Muller, 1971, Kennett, 1980), finite difference methods (Kelley, et al., 1976), and raytrace methods such as Chapman (1978) or Lawton and Howell (1992).

Most of these elastic wave modeling formulations amount to a direct simulation of the elastic wave equations using either finite difference, finite element, or spectral methods. Hence these methods do not formally use results like the Zoeppritz equations since they are implicitly contained in the elastic wave equations. Though they produce very realistic results, elastic wave methods are not popular because the results tend to be as difficult to interpret as real data and the algorithms do not typically allow effects to be turned on and off. Ray trace elastic methods, like

SYNTH (Lawton and Howell, 1992, Margrave and Foltinek, 1995), use Snell's law for ray paths and the Zoeppritz equations for amplitudes. As such, they are much more flexible than full elastic wave methods but tend to lack realism in ways that are mostly attributable to the raytracing.

The method presented here falls between these two approaches. Phase shift extrapolation replaces Snell's law raytracing but the Zoeppritz equations are still used explicitly. Furthermore, the phase shift extrapolation is implemented as a cascade on a computational grid, similar to that familiar from 1-D normal incidence seismogram theory (Waters, 1981). Each Fourier plane wave is independently propagated through the computational cascade which allows all possible multiples and converted modes to be computed. The result is greater realism than SYNTH but more flexibility than traditional elastic wave modeling. A method similar in intent to the one proposed here but limited to non-evanescent plane waves and equal traveltime layers was presented in Easley and Foltinek (1993).

THEORY OF 2-D ELASTIC SEISMOGRAM CONSTRUCTION BY PHASE SHIFT CASCADE METHOD

Basic Wave Equations

The elastic wave equation for a homogeneous medium is a vector equation of motion written as

$$\rho\ddot{\boldsymbol{u}} = (\lambda+\mu)\overline{\nabla}(\overline{\nabla}\cdot\boldsymbol{u}) + \mu\nabla^2\boldsymbol{u} \tag{1}$$

where $\boldsymbol{u}$ is a particle displacement vector, λ and μ are the Lame' elastic parameters and ρ is the density of material the wave is traveling through. By Helmholtz's theorem we represent the displacement field (Lay and Wallace, 1995, p.54) as

$$\boldsymbol{u} = \overline{\nabla}\phi + \overline{\nabla}\times\boldsymbol{\psi} = \boldsymbol{u}_p + \boldsymbol{u}_s \tag{2}$$

where ϕ is a curl-free scalar potential field $(\overline{\nabla}\times\phi = 0)$ and $\boldsymbol{\psi}$ is a divergenceless vector potential field $(\overline{\nabla}\cdot\boldsymbol{\psi} = 0)$. P-wave displacement $(\boldsymbol{u}_p)$ is obtained from $\overline{\nabla}\phi$ and S-wave displacement $(\boldsymbol{u}_s)$ from $\overline{\nabla}\times\boldsymbol{\psi}$. Substituting equation (2) into equation (1) and using the vector identity (Bath, 1984, p.9)

$$\nabla^2\boldsymbol{u} = \overline{\nabla}(\overline{\nabla}\cdot\boldsymbol{u}) - (\overline{\nabla}\times\overline{\nabla}\times\boldsymbol{u}) \tag{3}$$

allow us to separate the elastic wave equation into two wave equations for P-wave and S-wave potentials

$$\ddot{\phi} = \alpha^2 \nabla^2 \phi \tag{4}$$

where $$\alpha = \sqrt{\frac{\lambda + 2\mu}{\rho}} \tag{5}$$

and $$\ddot{\boldsymbol{\psi}} = \beta^2 \nabla^2 \boldsymbol{\psi} \tag{6}$$

where $$\beta = \sqrt{\frac{\mu}{\rho}}\,. \tag{7}$$

Equation (4) is a scalar wave equation for ϕ and uses the P-wave velocity, α. The vector wave equation in (5) has a vector solution $\boldsymbol{\psi}$ and uses β, the shear wave velocity. Thus, the potentials in the wave equation are separated into P and S components and each of which involves one wave velocity at a time. Therefore it is much simpler to solve the elastic wave equation using potentials for the elastic displacement than directly. Once the potentials are determined, displacements can be computed from equation (2).

Solutions for Potentials

In two dimensions with Cartesian coordinates (see Aki and Richards, 1980, p.128-129, for complete discussions), the vector potential for an SV-wave has only one component as $\boldsymbol{\psi} = (0, \psi(x,z,t), 0)$ with displacement

$$\boldsymbol{u}_s = \overline{\nabla} \times \boldsymbol{\phi} = (-\frac{\partial \psi}{\partial z}, 0, \frac{\partial \psi}{\partial x})\,. \tag{8}$$

When equation (8) is substituted into (6), the vector wave equation in (6) is reduced to a scalar form as

$$\ddot{\psi}(x,z,t) = \beta^2 \nabla^2 \psi(x,z,t)\,. \tag{9}$$

For a P-wave, $\phi = \phi(x,z,t)$ and the displacement is

$$\boldsymbol{u}_p = \overline{\nabla} \phi = (\frac{\partial \phi}{\partial x}, 0, \frac{\partial \phi}{\partial z})\,. \tag{10}$$

We will now develop the solution to equation (4) using a Fourier method. We represent the P-wave potential as a Fourier plane wave superposition by

$$\phi(x,z,t) = \left(\tfrac{1}{2\pi}\right)^2 \int_{-\infty}^{\infty} \Phi(k_x, z, \omega) e^{i(k_x x - \omega t)} dk_x d\omega \tag{11}$$

where ω is an angular frequency and k_x is an angular horizontal wavenumber. In this expression, Φ is the Fourier spectrum of ϕ and represents the contribution of each Fourier plane wave, $e^{i(k_x x - \omega t)}$, to the construction of ϕ. We can determine an

equation for Φ by substituting equation (11) into equation (4). After some manipulation and assuming α is constant, we obtain

$$\int_{-\infty}^{\infty}\int[-k_x^2\Phi + \frac{\partial^2\Phi}{\partial z^2} + \frac{\omega^2}{\alpha^2}\Phi]e^{i(k_x x-\omega t)}dk_x d\omega = 0 . \tag{12}$$

This can only be satisfied for all k_x and ω, by requiring the term in brackets to vanish. Thus

$$\frac{\partial^2\Phi}{\partial z^2} = -k_z^2\Phi \tag{13}$$

where k_z is an angular vertical wavenumber given by

$$k_z^2 = \frac{\omega^2}{\alpha^2} - k_x^2 . \tag{14}$$

Equation (13) is an ordinary differential equation for the spectrum Φ. Its general solution can be verified by substitution to be

$$\Phi(k_x, z, \omega) = A(k_x, \omega)e^{ik_z z} + B(k_x, \omega)e^{-ik_z z} \tag{15}$$

where k_z is the positive square root of (14). Here, A and B represent the strengths of waves traveling in the +z direction (downward) and –z direction (upward) respectively. Since the wave equation is a second order differential equation, we expect two such undetermined quantities which must be calculated from the boundary conditions for a particular problem. Finally, we obtain a general solution for the P-wave potential in equation (4) by substituting equation (15) into (11) to get

$$\phi(x,z,t) = \left(\tfrac{1}{2\pi}\right)^2 \int_{-\infty}^{\infty}\int (A(k_x, \omega)e^{ik_z z} + B(k_x, \omega)e^{-ik_z z})e^{i(k_x x-\omega t)}dk_x d\omega . \tag{16}$$

Note that we follow the choice of sign convention for Fourier transforms used in solving wave-propagation problems relevant to seismology by Aki and Richards,1980 (p.129-130). In equation (16), the exponential term, for positive real k_x and k_z, is a plane wave propagating in the direction of increasing x and z. When k_z is imaginary, the exponential in (16) changes from a complex sinusoid to a growing or decaying real exponential. Therefore the sign of the imaginary k_z is chosen to be positive so that these waves are not physically increasing with vertical distance. Plane waves associated with this imaginary k_z are called evanescent waves. Thus, in summary, k_z is given by

$$k_z = \begin{cases} \sqrt{\dfrac{\omega^2}{\alpha^2} - k_x^2} & , \quad \dfrac{\omega^2}{\alpha^2} \geq k_x^2 \\ i\sqrt{k_x^2 - \dfrac{\omega^2}{\alpha^2}} & , \quad \dfrac{\omega^2}{\alpha^2} < k_x^2 \end{cases}. \tag{17}$$

In a similar process, equation (6) can be solved for the S-wave potential, $\psi(x,z,t)$, and expressed in the Fourier domain as:

$$\Psi(k_x, z, \omega) = C(k_x, \omega)e^{ik_z z} + D(k_x, \omega)e^{-ik_z z} \tag{18}$$

and in the space-time domain as

$$\psi(x,z,t) = \left(\tfrac{1}{2\pi}\right)^2 \int_{-\infty}^{\infty}\int (C(k_x,\omega)e^{ik_z z} + D(k_x,\omega)e^{-ik_z z})e^{i(k_x x - \omega t)}dk_x d\omega \tag{19}$$

where k_z has the same interpretation as for the P-wave in equation (17), only the velocity changes from α to β as

$$k_z = \begin{cases} \sqrt{\dfrac{\omega^2}{\beta^2} - k_x^2} & , \quad \dfrac{\omega^2}{\beta^2} \geq k_x^2 \\ i\sqrt{k_x^2 - \dfrac{\omega^2}{\beta^2}} & , \quad \dfrac{\omega^2}{\beta^2} < k_x^2 \end{cases}. \tag{20}$$

Consider a monochromatic plane P wave at a depth z in a homogeneous medium, $\Phi(k_x, z, \omega)$, equation (15) suggests it contains two wavefields, downgoing and upgoing:

$$\Phi(k_x, z, \omega) = \Phi_d(k_x, z, \omega) + \Phi_u(k_x, z, \omega) \tag{21}$$

where Φ_d is the first term associated with $+k_z$ in equation (15) and Φ_u the second term with $-k_z$. If we substitute $z=z+\Delta z-\Delta z$ into the right-hand-side of equation (15) we can trace each wave component of $\Phi(k_x, z, \omega)$ upward or downward in depth (and backward or forward in time), over a depth interval Δz. Suppose we want to express histories of both wave components, we need to arrange $\Phi(k_x, z, \omega)$ in terms of downcoming waves from above, $\Phi_{dc}(z-\Delta z)$, and upcoming wave from below, $\Phi_{uc}(z-\Delta z)$. After some basic manipulations of equations (15) and (21), the history of a plane P wave at a depth z is restored to predict $\Phi(k_x, z, \omega)$ as

$$\Phi(k_x, z, \omega) = \Phi_{dc}(z-\Delta z)e^{ik_z \Delta z} + \Phi_{uc}(z+\Delta z)e^{ik_z \Delta z}. \tag{22}$$

On the other hand, a backward derivation is obtained to bring back $\Phi(k_x, z, \omega)$ in terms of a downgoing wave at $z+\Delta z$ and an upgoing wave at $z-\Delta z$ as

$$\Phi(k_x, z, \omega) = \Phi_{dg}(z + \Delta z)e^{-ik_z \Delta z} + \Phi_{ug}(z - \Delta z)e^{-ik_z \Delta z}, \tag{23}$$

which has been used reciprocally to equation (22) in phase shift migration (Gazdag, 1978).

The term $e^{ik_z \Delta z}$ in equation (22) is called the phase shift extrapolator which delays the phase of $\Phi_d(z)$ for $\Phi_{dg}(z + \Delta z)$ and of $\Phi_u(z)$ for $\Phi_{ug}(z - \Delta z)$, according to a depth interval Δz. Equation (22) is then used to extrapolate a downgoing component from $z + \Delta z$ and an upgoing component from $z - \Delta z$ for a forward modeling of $\Phi(k_x, z, \omega)$. The forward phase-shift equation for an S wave is achieved by the same consideration from equation (18) and written as

$$\Psi(k_x, z, \omega) = \Psi_{dc}(z - \Delta z)e^{ik_z \Delta z} + \Psi_{uc}(z + \Delta z)e^{ik_z \Delta z} \tag{24}$$

where

$$\Psi(k_x, z, \omega) = \Psi_d(k_x, z, \omega) + \Psi_u(k_x, z, \omega) \tag{25}$$

and k_z for S wave is given by equation (20).

Scattering Considerations

In the phase-shift cascade method, we use equation (22) for a P-wave and equation (24) for an S wave to recursively extrapolate each Fourier plane wave from a surface source downward to reflectors and from reflectors upward back to the surface. Four possible wave fields in equation (15) and (18), corresponding to up and downgoing P and S potentials, are maintained along the calculation path. At every interface, the complex amplitudes $A, B, C,$ and D have to be redetermined by four boundary conditions for four unknowns. Fortunately, this work has been formulated into a set of amplitude ratios of resulting waves to their incident waves. These ratios are called reflection and transmission coefficients. In terms of displacements, the Zoeppritz equations are derived for these 16 coefficients in a P-SV plane wave system at a plane interface (Aki and Richard, p.144). The system consists of four possible incident waves and t heir four resulting scattered waves as shown in Figure 1.

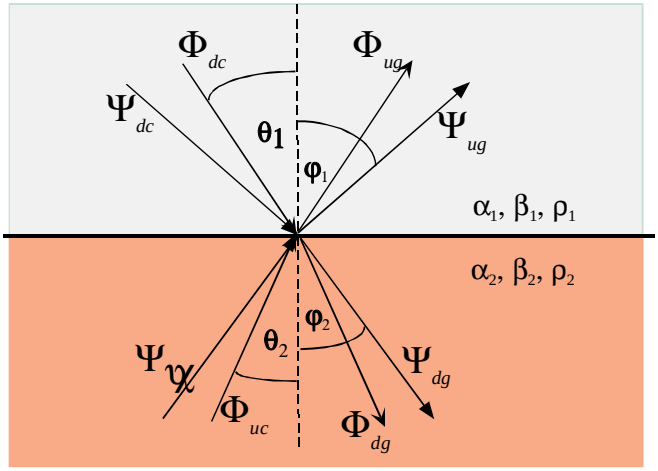

Figure 1. Incoming and outgoing P and S potentials at a computation node

In figure(1), we denote "*d*" for down and "*u*" for up in the directions of propagation, "*c*" for coming or incident waves and "*g*" for going or resultant waves as their current status. In order to solve this P-SV problem, these four boundary conditions are applied for each incident wave:

continuity of vertical displacement : $$\sum_{\text{medium1}} U_z = \sum_{\text{medium2}} U_z \tag{26}$$

continuity of shear displacement : $$\sum_{\text{medium1}} U_x = \sum_{\text{medium2}} U_x \tag{27}$$

continuity of normal stress : $$\sum_{\text{medium1}} \sigma_{zz} = \sum_{\text{medium2}} \sigma_{zz} \tag{28}$$

continuity of tangential stress : $$\sum_{\text{medium1}} \sigma_{zx} = \sum_{\text{medium2}} \sigma_{zx} \tag{29}$$

where U symbolizes a displacement magnitude for a monochromatic component of the Fourier transform for u. The complete results for all incident waves and full discussion are given in Aki and Richards, p.144-151. The reflection coefficients are modified and summarized in a scattering matrix in the following text. The Zoeppritz equations determine the displacement amplitudes of the reflected and refracted plane waves. In order to apply them to the wave potentials we are working with, we use an amplitude relation between displacement and potential given by Aki and Richards (p.139) as

$$A_U = \frac{\omega}{\alpha} A_\Phi = \frac{\omega}{\beta} A_\Psi \tag{30}$$

where A_U, A_Φ and A_Ψ are the amplitudes of total displacement, P-wave potential and S-wave potential, respectively, for a plane wave. Equation (30) can be obtained by taking a spatial derivative of the wave potential for the displacement as written in equation (8) and (10) of P and S waves. Then the vector magnitude of displacement is computed and using equation (14) gives the relation in (30). Since the reflection coefficients are amplitude ratios of scattering waves to incident waves, we can modify the coefficients obtained from Zoeppritz equations to be for potential by multiplying by a ratio of a scattering velocity to an incident velocity. Let subscripts i and s indicate a type (P or S) of an incident and a scattered waves, respectively and v is a velocity $(\alpha_1, \alpha_2, \beta_1, \text{and}, \beta_2)$ of the subscripted wave for the medium 1 or 2 in which it is traveling. Then a general relation between reflection or transmission coefficients for potential and displacement can be written as

$$R_{is}(\Phi) = \frac{v_s}{v_i} R_{is}(U) . \tag{31}$$

Thus the algorithm is completely in terms of elastic potentials and displacements are only computed at the end, if desired.

Now we express the relation between four outgoing potential wavefields (on the left-hand side of the equation) and four incoming potential wavefields at an interface by a matrix equation as

$$\begin{bmatrix} \Phi_{dg} \\ \Phi_{ug} \\ \Psi_{dg} \\ \Psi_{ug} \end{bmatrix} = \begin{bmatrix} T_{pp} & R^{-}_{pp} & T_{sp} & R^{-}_{sp} \\ R_{pp} & T^{-}_{pp} & R_{sp} & T^{-}_{sp} \\ T_{ps} & R^{-}_{ps} & T_{ss} & R^{-}_{ss} \\ R_{ps} & T^{-}_{ps} & R_{ss} & T^{-}_{ss} \end{bmatrix} \begin{bmatrix} \Phi_{dc} \\ \Phi_{uc} \\ \Psi_{dc} \\ \Psi_{uc} \end{bmatrix}. \tag{32}$$

In this expression, T_{sp} is, for example, the transmission coefficient for an S wave converting to a P wave where the S wave is an incident from above and T^{-}_{sp} is similar except that the S wave is incident from below. The scattering matrix summarizes all possible reflection and transmission coefficients in a (4×4) matrix where each row represents four contributions from the four incident waves to a particular type of resultant wave. This explicit formulation allows us to acquire various desired physical results with selective contributions. This is a major advantage of this algorithm over other wave equation based methods. For example, if we want to have merely P and converted primaries and suppress all multiples, we shall set those reflection coefficients of the upcoming waves in scattering matrix to zero, i.e. equation (32) becomes

$$\begin{bmatrix} \Phi_{dg} \\ \Phi_{ug} \\ \Psi_{dg} \\ \Psi_{ug} \end{bmatrix} = \begin{bmatrix} T_{pp} & 0 & T_{sp} & 0 \\ R_{pp} & T^{-}_{pp} & R_{sp} & T^{-}_{sp} \\ T_{ps} & 0 & T_{ss} & 0 \\ R_{ps} & T^{-}_{ps} & R_{ss} & T^{-}_{ss} \end{bmatrix} \begin{bmatrix} \Phi_{dc} \\ \Phi_{uc} \\ \Psi_{dc} \\ \Psi_{uc} \end{bmatrix}. \tag{33}$$

If mode conversions are not desired:

$$\begin{bmatrix} \Phi_{dg} \\ \Phi_{ug} \\ \Psi_{dg} \\ \Psi_{ug} \end{bmatrix} = \begin{bmatrix} T_{pp} & R^{-}_{pp} & 0 & 0 \\ R_{pp} & T^{-}_{pp} & 0 & 0 \\ 0 & 0 & T_{ss} & R^{-}_{ss} \\ 0 & 0 & R_{ss} & T^{-}_{ss} \end{bmatrix} \begin{bmatrix} \Phi_{dc} \\ \Phi_{uc} \\ \Psi_{dc} \\ \Psi_{uc} \end{bmatrix}. \tag{34}$$

If, at some nodes, we want primaries without mode conversion, we combine equation (33) and (34) getting

$$\begin{bmatrix} \Phi_{dg} \\ \Phi_{ug} \\ \Psi_{dg} \\ \Psi_{ug} \end{bmatrix} = \begin{bmatrix} T_{pp} & 0 & 0 & 0 \\ R_{pp} & T^{-}_{pp} & 0 & 0 \\ 0 & 0 & T_{ss} & 0 \\ 0 & 0 & R_{ss} & T^{-}_{ss} \end{bmatrix} \begin{bmatrix} \Phi_{dc} \\ \Phi_{uc} \\ \Psi_{dc} \\ \Psi_{uc} \end{bmatrix}. \tag{35}$$

In case that we require P-S converted primaries only, we may use

$$\begin{bmatrix} \Phi_{dg} \\ \Phi_{ug} \\ \Psi_{dg} \\ \Psi_{ug} \end{bmatrix} = \begin{bmatrix} T_{pp} & 0 & 0 & 0 \\ 0 & 0 & 0 & 0 \\ 0 & 0 & 0 & 0 \\ R_{ps} & 0 & 0 & T_{ss}^{-} \end{bmatrix} \begin{bmatrix} \Phi_{dc} \\ \Phi_{uc} \\ \Psi_{dc} \\ \Psi_{uc} \end{bmatrix}. \tag{36}$$

There are many other possibilities of physical effects that we can isolate or exclude by similar manipulations of the scattering matrix.

Source Representation

In the real world, it is impractical to generate plane waves but, mathematically, it is difficult to deal directly with spherical waves. Fortunately, we can use Fourier analysis to decompose the spherical wave of the real world into a sum of harmonic plane waves in our numerical world. However, the boundless span with constant amplitude of a harmonic plane wave would give us an enormous energy, which is not physical. For a realistic source, to have finite energy, we implement the Weyl integral (Brekhovskikh, 1980, p.228-231). It describes a point source in a three-dimensional spectral domain by defining a radial-dependent amplitude attenuation for each plane wave for a harmonic spherical wave expansion. The potential for a spherical wave emanating from a point source in a homogeneous material is given by the Weyl integral:

$$\frac{e^{i(kR-\omega t)}}{R} = \frac{i}{2\pi} \int \int_{-\infty}^{\infty} e^{i(k_x x + k_y y \pm k_z z - \omega t)} \frac{dk_x dk_y}{k_z} \tag{37}$$

where $R = \sqrt{x^2 + y^2 + z^2}$ and $k = \sqrt{k_x^2 + k_y^2 + k_z^2}$. The plus or minus sign of k_z corresponds to direction of wave propagation in positive or negative depth, respectively, as discussed earlier.

A pulsed spherical wave is acquired by multiplying a harmonic spherical wave in this expression with a complex wavelet spectrum and summing harmonic spherical waves in equation (37) over frequency (Tygel and Hubral, 1987, p.40). It is equivalent to convolving an impulsive spherical wave with a wavelet in the time domain. In two dimensions, we can summarize an expression for a wave potential for a pulsed point source in a form parallel to our wave solution (16) by setting $k_y = 0$

$$w(t) * \int_{-\infty}^{\infty} \frac{e^{i(kr-\omega t)}}{\mathrm{r}} d\omega = \left(\frac{1}{2\pi} \right)^2 \int_{-\infty}^{\infty} W(\omega) \int_{-\infty}^{\infty} \left(\frac{i}{k_z} e^{i(k_x x + k_z z - \omega t)} + \frac{i}{k_z} e^{i(k_x x - k_z z - \omega t)} \right) dk_x d\omega . \tag{38}$$

where we have explicitly taken an inverse Fourier transform over ω. Substitute $k = \frac{\omega}{v}$ in the exponential argument on the left-hand side of this equation and the integration becomes an impulsive cylindrical wave function:

$$w(t)*\frac{\delta(r/v-t)}{r}=\left(\frac{1}{2\pi}\right)^2\int_{-\infty}^{\infty}W(\omega)\int_{-\infty}^{\infty}\left(\frac{i}{k_z}e^{i(k_x x+k_z z-\omega t)}+\frac{i}{k_z}e^{i(k_x x-k_z z-\omega t)}\right)dk_x d\omega \qquad (39)$$

where $w(t)$ is a wavelet function, $W(\omega)$ is a wavelet spectrum, $r=\sqrt{x^2+z^2}$ and $k=\sqrt{k_x^2+k_z^2}$. Compare equation (38) to our wave solutions in (16) for P wave and (19) for S wave. If we evaluate a pulsed point source for a cylindrical P-wave at the surface $(z=0)$ and pay no attention to the upgoing waves above surface, then we will have

$$\phi(x,0,t)=w(t)*\frac{\delta(x/v-t)}{x}, \qquad (40)$$

$$\psi(x,0,t)=0, \qquad (41)$$

$$\Psi(k_x,0,\omega)=0, \qquad (C=0,\ D=0), \qquad (42)$$

and

$$\Phi(k_x,0,\omega)=A(k_x,\omega)e^{i(k_x x-\omega t)}, \qquad (B=0), \qquad (43)$$

where

$$A(k_x,\omega)\ =\ W(\omega)S(k_x,\omega)\ =\ \frac{i}{k_{z1}}W(\omega) \qquad (44)$$

and a source term

$$S(k_x,\omega)=\ \frac{i}{k_{z1}}\ =\ \frac{i}{\sqrt{\frac{\omega^2}{\alpha_1^2}-k_x^2}} \qquad (45)$$

for a point source. Therefore, the boundary condition on Φ for a point source in 2-D is:

$$\Phi(k_x,0,\omega)\ =\ \frac{i}{k_{z1}}W(\omega)e^{i(k_x x-\omega t)} \qquad (46)$$

The source term is evaluated at the surface for this boundary condition. Therefore the P-wave velocity in (45) is α_1 for the layer that the source is located in. It is, then, independent of depth while the initial plane wave propagates up and down through the media. The wavelet term $W(\omega)$ depends only on frequency. So these two functions can simply multiply the output (k_x,ω) spectrum at the end of the extrapolation process. We can begin with an S-wave point source, which with a similar consideration, we get a source term as

$$\Psi(k_x,0,\omega)\ =\ \frac{i}{k_{z1}}W(\omega)e^{i(k_x x-\omega t)}. \qquad (47)$$

where the velocity in equation (45) for k_{z1} is β_1. In case that both P and S source are required, the source term is a combination of equation (46) and (47).

The derivation of equation (37) suggests there must be inhomogeneous plane waves propagating in the horizontal plane with a wavelength, which converges to zero, and most rapidly attenuating in the vertical direction. Such waves correspond to a complex angle of incidence in the integral range of the polar form (Bath, 1984, p.191). They have to be included for this expansion of spherical wave emanating from a point source into plane waves. This type of wave was referred to earlier as an evanescent wave, in the discussion of imaginary vertical wavenumber, equation (17). They are also known, in time domain, under the name of head waves, conical waves or, sometimes, merely refractions. They appear in a shot record after a critical distance where the waves are refracted at 90 degree. Our method produces these waves as will be shown in the experimental section.

Algorithm

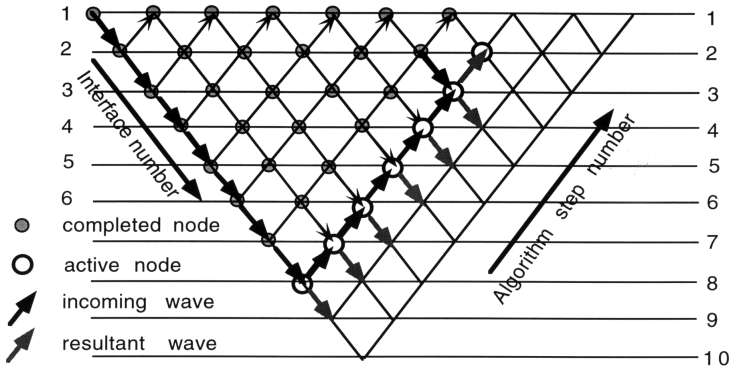

Figure 2. Plane-wave cascade

The plane-wave cascade in Figure 2 illustrates how we track down the travel path of a plane wave to reflectors and determine their physical interactions along every possible way that waves can propagate back to the receiver. Waters (1981, p.131) used this diagram to describe a 1-D normal incidence seismogram method.

In the first step of our calculation, a compressional point source is initiated at $z = 0$ in (k_x, ω) plane, and yields $\Phi(k_x, z = 0, \omega)$ in equation (46). On the computational grid in Figure 2, it is set up at (interface1, step1) which we shall call node(1,1). The output $\Phi'_{uc}(z = 0)$ and $\Psi'_{uc}(z = 0)$ in (k_x, ω) coordinates are zeros at this beginning node(1,1). The extrapolator in equation (22) is employed to downward continue each (k_x, ω) component of Φ to the second interface, node(2,1), by Δz_1. In order to propagate a wavefield across a solid-solid interface, four boundary conditions in equation (26)-(29) are required. So equation (32) is applied to the potentials at node(2,1) setting

$$\Phi_{dc} = \Phi(k_x, \Delta z_1, \omega) \tag{48}$$

and

$$\Phi_{uc} = \Psi_{dc} = \Psi_{uc} = 0\,. \tag{49}$$

Thus the four outgoing wavefields are established and ready to be propagated up and down separately to be incoming wavefields of the next two nodes, (3,1) and (1,2). In

this triangular grid, we trace down one node along the left boundary and ,then, up to cover every node along the upgoing path to the surface before coming back down to the bottommost and repeating the procedure again (Figure 2). At each step in the cascade, events arrive at the surface (interface1), are summed into the output *f-k* spectra (Φ' and Ψ').

Normally, the wavefront aperture of a cylindrical wave in the lower layer is smaller than (or maintains the same as) in the upper layer when it penetrates through a boundary according to an associated critical angle or a maximum offset required in modeling. Therefore we can reduce computation time, aimed for reflections, by compressing the cylindrical wavefront as the wave goes deeper. In this manner, the plane wave expansion is limited within a certain ray parameter which may vary with depth. We used raytracing for PP-wave to estimate a suitable ray parameter range for every reflection in a model. Then the calculation zone in the *f-k* plane for each layer is minimized. PS raytracing can replace PP for mode conversion priority in any depth.

When every element of P- and S-potential spectra, $\Phi'_{ucf}(k_x,0,\omega)$ and $\Psi'_{uc}(k_x,0,\omega)$, are computed at the surface, we can add surface reflections for free-surface effects and/or convert them to displacements using

$$\boldsymbol{U} = (k_x\Phi' - k_z\Psi')\hat{\boldsymbol{l}} + (k_z\Phi' + k_x\Psi')\hat{\boldsymbol{n}} \tag{50}$$

which is developed from equation (2) using equation (15) and (18). In this expression $\hat{\boldsymbol{l}}$ is a unit vector in the ***x*** direction and $\hat{\boldsymbol{n}}$ in the ***z*** direction.

In summary, after evaluating the wavefield for a P-wave point source at the surface, we extrapolate every plane wave component downward across arbitrary thickness homogeneous layers to reflectors via a computation diagram in Figure 3 which produces every possible multiple and converted mode within the grid. We compute the reflections, transmissions and conversions at interfaces using modified-for-potential Zoeppritz equations. All four incident waves are used to generate the four resulting waves for a full solution. At this stage, we can include or exclude multiples and mode conversions with a properly reformed scattering matrix as illustrated in equation (33) to (36). This physical effect control can be depth dependent by taking advantage of griding calculation. The upgoing P and S waves from reflectors are propagated upward back to the surface, again, by applying the extrapolators and boundary conditions. Then the output component in the *f-k* domain is determined as a sum of the multiple arrivals of an individual wavefield at the surface. If freesurface effects are required, we add P- and S- potential reflections to the output plane before displacement conversions (again, if desired) and inverse Fourier transform to achieve a final result in space-time domain.

RESULTS AND DISCUSSIONS

We used the three synthetic layered models in Figure 3 to test the program. There are two single-interface models with the same two media but in alternate order. The third model has more layers and produces more complicated results. The density for every layer in all models is constant (1.00g/cm^3).

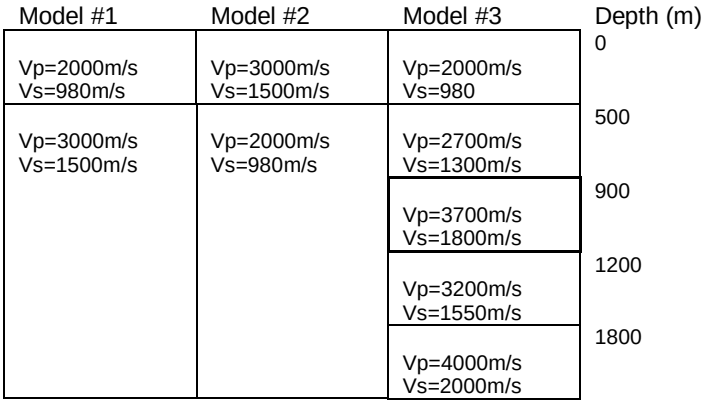

Figure 3. Configuration of the three simple models

The time sample rate for modeling was 4ms and the trace interval was 25m. Maximum offsets for model #1 and #2 was 3200m and for model #3 2000m. An appropriate range of ray parameter is evaluated for every depth in these three models. A compressional wavelet with a Gaussian frequency spectrum was used as a source.

The results for PS waves in term of potential and horizontal displacement have polarity reversal at the negative offset in every model, Figure 4(b), 4(d), 5(b) and 5(d).

The synthetic potentials and displacements from model #1, which has a lower velocity layer on top (vp1<vs2<vp2), show headwaves in both PP and PS reflections as marked in Figure 4(a), 4(b), 4(c) and 4(d). The results from model #2 which has a higher velocity layer on top, do not show headwaves, Figure 5(a) 5(b), 5(c) and 5(d). There are phase changes in supercritical reflections of the results from model#1, Figure 4. These imply the method produces headwaves which correspond to ray parameters within our model range because the Zoeppritz equations give the correct amplitude and phases and plane wave superposition then correctly constructs such waves.

Synthetic-cylindrical-reflection coefficients can be obtained by dividing actual reflections by reference reflections. We can compute a reference PP wave by the same procedure and parameters as the actual wave but only with Rpp=1 (and Rps=1 for a reference PS) at a particular reflector, for every plane wave. We then raytrace travel times for the reflection and interpolate its amplitude for the actual wave and the reference waves. We applied two amplitude determination methods at this stage, Hilbert envelope and Sinc-function interpolations. The Hibert envelope, due to the wavelet with Guassian frequency spectrum, gives data magnitude at the specific travel time. The Sinc function interpolates a trending amplitude which represents only the real part of the complex amplitude. The cylindrical reflection coefficient is then estimated by dividing the actual amplitude by the reference amplitude. Due to two different amplitude extractions, we get both amplitude and instantaneous phase information or both real and imaginary parts of the constructed reflection coefficients as plotted together with the analytic results from Zoeppritz equations at different

offsets in Figure 4 (a) and (b) for model#1. The phase information are plotted in the multiplication of π radian and shifted down 0.4π in order to be shown in the same figure as the amplitude information. For model#2, there is only real part of reflection coefficient from Zoeppritz equations as shown in Figure 6. There are correlation trends in every case but the synthetic coefficient from model#1 are shifted to farther offset and smoothed compared to plane wave coefficients. Amplitude maxima associated with critical angles appear shifted to farther offsets than predicted from the Zoeppritz equations. This has been observed and discussed previousely by Rendleman and Levin (1988) and Krail and Brysk (1983).

The potential responses from the third model are PP primaries plus multiples, PP primaries, PS primaries plus multiples and PS primaries displayed in Figure 8(a), 8(b), 8(c) and 8(d), respectively. There are many realistic effects in these figures which will be the subject of future research.

We are pleased with the results we have got at this stage. We are working for a more efficient program that will be more flexible and faster. As for the model #3, the code calculated for 275 wavenumbers and 348 frequencies through 5 interfaces and 5 algorithm steps within 160seconds. S-wave sources are easily done. The extension to 3-D is very possible. It could also be extended to an attenuating medium by using complex velocities and anisotropy case using velocity depending on ray parameters.

CONCLUSIONS

This method produces theoretically correct synthetic amplitudes and travel times with head waves for potential and displacement seismograms. Together with an economic computation design, it is fast and stable. Multiples and mode conversions are controlled via the scattering matrix. The manipulations can vary with depth. The cylindrical reflection coefficients are obtainable.

The algorithm is intuitive, reliable and very extendible into many more complicated problems. Yet it gives a realistic results. It gains advantages from both main modeling categories, raytracing and wave equation. This method is a good tool to conveniently study various complicated cases that need insightful and realistic modeling, such as thin layers with high impedance contrast. Anisotropic and anelastic cases are easily to handle in FK domain by this method. It can also be extended to 3-D simulation.

ACKNOWLEDGEMENT

We would like to kindly thank the CREWES sponsors and Thai government for all of their support. Dr. Ed Krebes and Dr. Don Lawton provided valuable technical suggestions. We also acknowledge every comment, suggestion and discussion of CREWES staffs and students. Special thanks to Kengan Fang for providing a cozy working place for these two months.

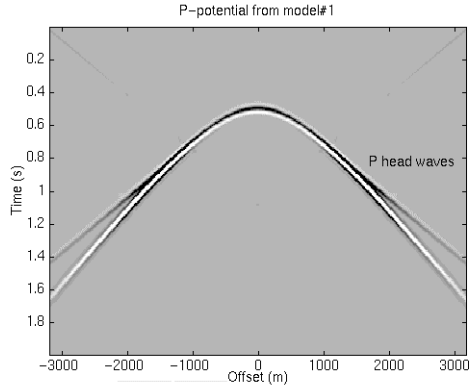

(a) P potential

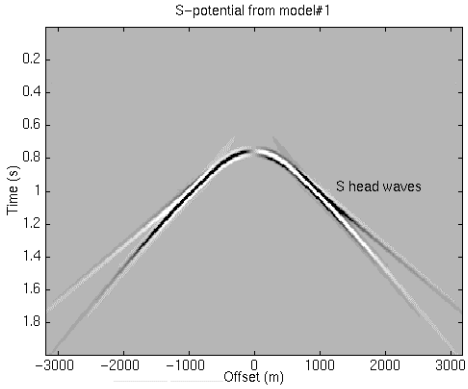

(b) S potential

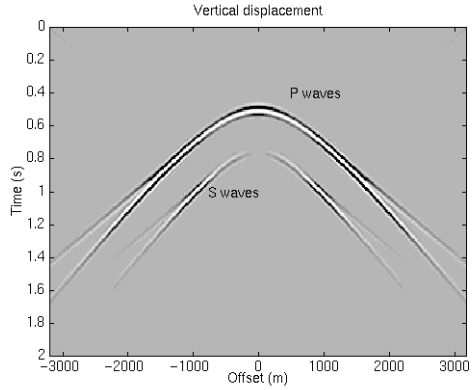

(c) Vertical displacement

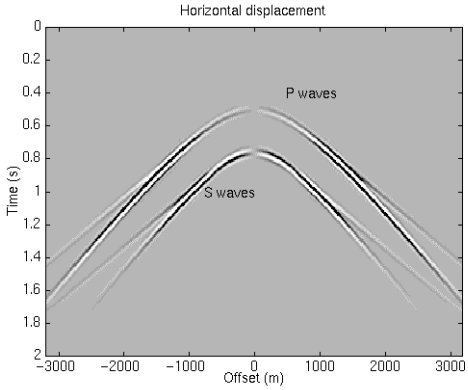

(d) Horizontal displacement

Figure 3. Potential and displacement responses from model #1

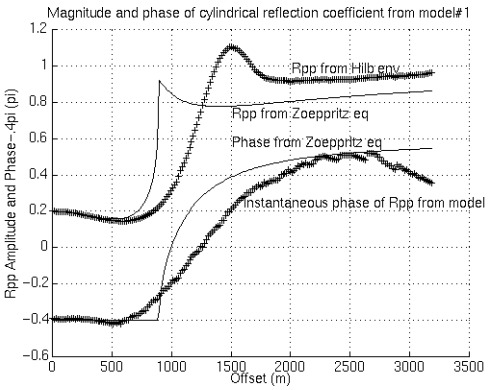

(a) From Hilbert envelope method

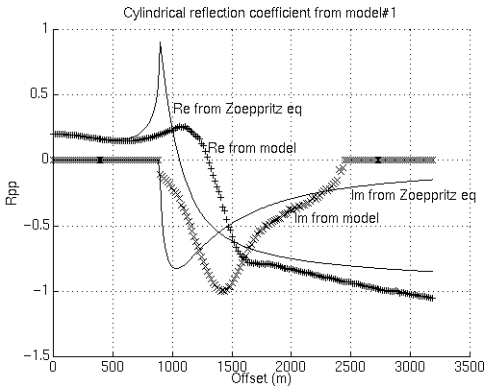

(b) From interpolation

Figure 4. Extracted reflection coefficients from synthetic data of model #1

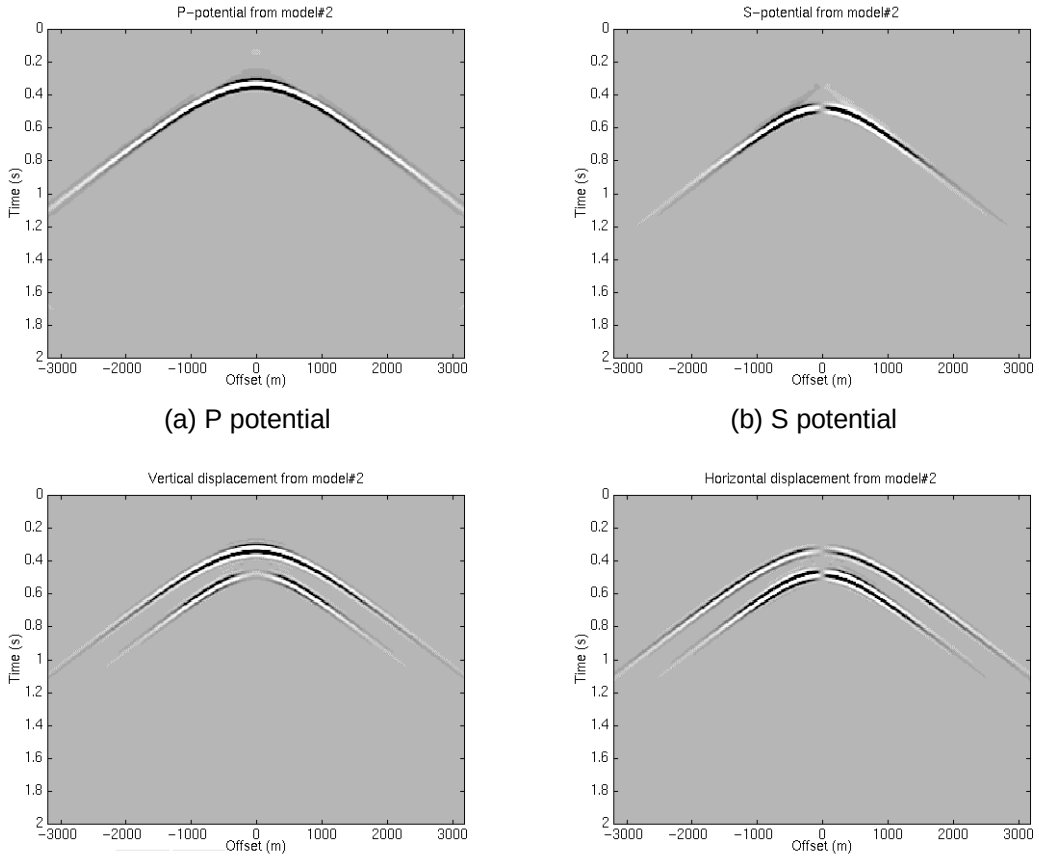

(a) P potential (b) S potential

(c) Vertical displacement (d) Horizontal displacement

Figure 5. Potential and displacement responses from model #2

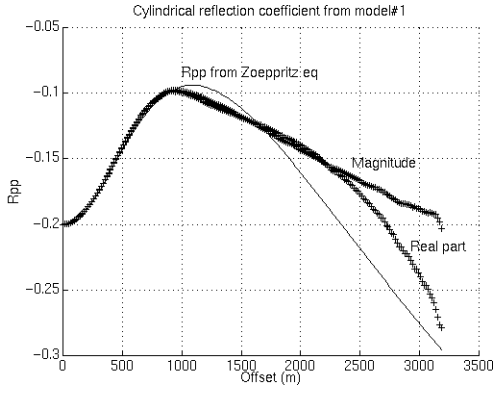

Figure 6. Extracted reflection coefficients from synthetic data of model #2

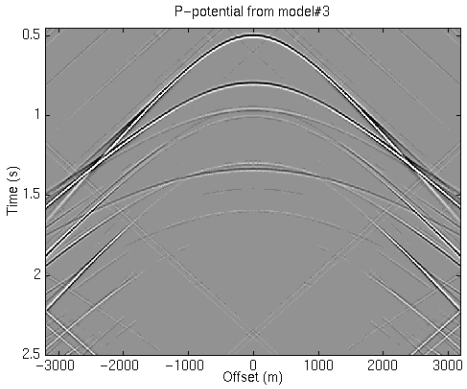

(a) P-wave primaries plus multiples

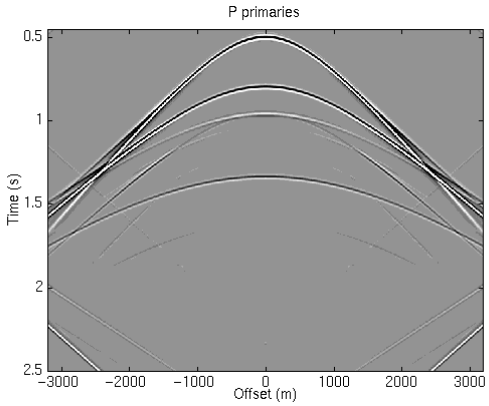

(b) P-wave Primaries

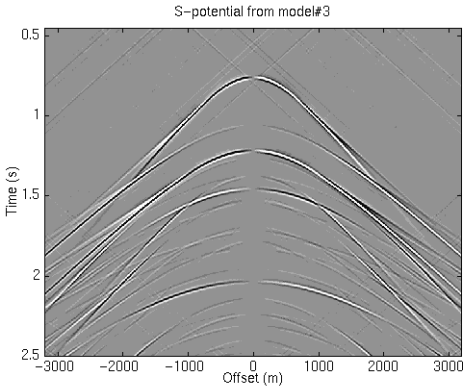

(c) S-wave primaries plus multiples

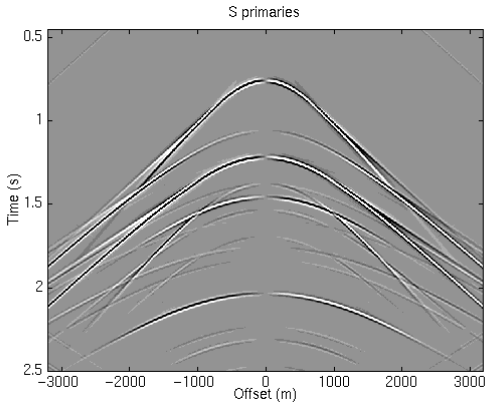

(d) S-wave Primaries

Figure 7. PP and PS reflections from model #3

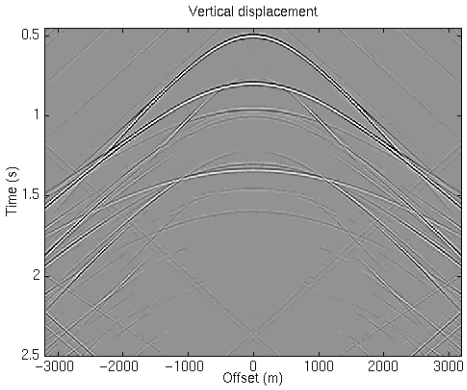

(a) Primaries plus multiples in vertical component

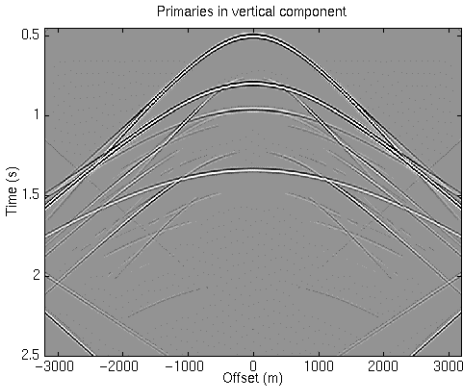

(b) Primaries only in vertical component

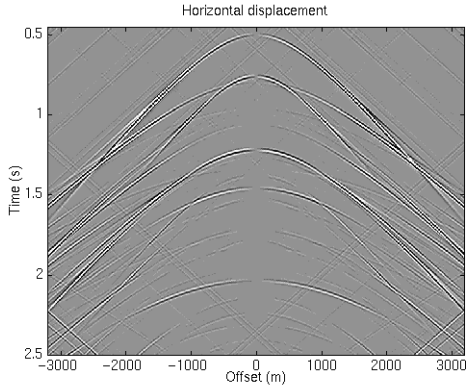

(c) Primaries plus multiples in horizontal component

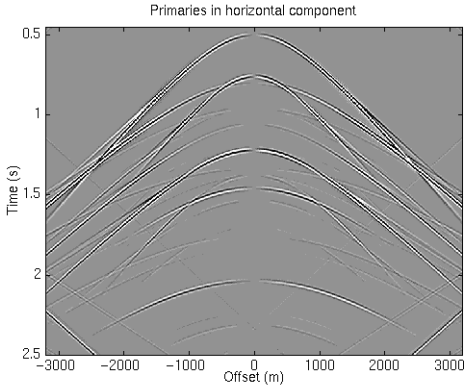

(d) Primaries only in horizontal component

Figure 8. Vertical and Horizontal displacements from model #3

References:

Aki, K., and Richards, P.G., 1980, Quantitative Seismology, Theory and Methods, W.H. Freeman and Company.

Bath, M. and Berkout, A.J., 1984, Mathematical aspect of seismology, Seismic exploration, **17**, Geophysical Press.

Brekhovskikh, L.M., 1980, Waves in layered media, Academic Press.

Chapman, C. H., 1978, A new method for computing seismograms: G. J. R. A. S., **54**, 481-518.

Easley, D.T., and Foltinek, D.S., 1993, Synthetic seismogram for P and S waves using the Goupillaud model, 1993 Annual Research Report of The CREWES Project.

Frasier, C.W., 1980, A new time domain reflection seismogram, presented at 12th Offshore Technology Conference in Houston, Tex., May5-8.

Fuchs, K., and Muller, G., 1971, Computation of synthetic seismograms with the reflectivity method and comparison with observations: G. J. R. A. S., **23**, 417-433.

Kelly, K. R., Ward, R. W., and Treitel, S., 1976, Synthetic seismograms: A finite-difference approach: Geophysics, **41,** 2-27.

Kennett, B.L.N., 1980, Seismic waves in a stratified half space-II. Theoretical seismograms: G.J.R.A.S., **61**, 1-10.

Krail, P.M., and Brysk, H., 1983, Reflection of spherical seismic waves in elastic layered media: Geophysics, **48**, 655-664.

Lawton, D.C., and Howell, T.C., 1992, P-P and P-SV synthetic stacks, Expanded Abstract, 62nd SEG Annual International Meeting, October 25-29, New Orleans, USA, 1344-1347.

Lay, T., and Wallace, T. C., 1995, Modern global seismology, Acadamic Press.

Margrave, G.F., and Foltinek, D.S., 1995, Synthetic P-P and P-SV cross sections, 1995 Annual Research Report of The CREWES Project.

Rendleman, C.A., and Levin, F.K., 1988, Reflection maxima for reflection from single interfaces: Gophysics, **53**, 271-275.

Sheriff, R.E. and Geldard, L.P., 1995, Exploration seismology, Cambridge University Press.

Silawongsawat, C., and Margrave, G.F., 1996, Multiple generation in normal incidence synthetic seismograms, 1996 Annual Research Report of The CREWES Project.

Tygel, M., and Hubral, P., 1987, Transient waves in layered media, Elsevier.

Waters, K.H., 1992, Reflection Seismology: A tool for energy resource exploration, 3rd edition, Krieger Publishing Co..